

8. ABRAHAM, S. C., KEVE, E. T.: *Ferroelectrics* **2**, 129 (1971).
9. KEVE, E. T., BYE, K. L., WHIPPS, P. W., ANNIS, A. D.: *Ferroelectrics* **3**, 39 (1971).
10. AIZU, K.: *J. Phys. Soc. Japan* **34**, 121 (1973).
11. AIZU, K.: *Phys. Rev. B* **2**, 754 (1970).
12. GOLDSMITH, G. J.: *Bull. Am. Phys. Soc.* **1**, 322 (1956).
13. WEIDER, H. H.: *J. Appl. Phys.* **30**, 1010 (1959).
14. HAINSWORTH, F. N., PETCH, H. E.: *Can. J. Phys.* **44**, 3083 (1966).
15. BIRSS, R. R.: *Symmetry and magnetism*. Amsterdam: North Holland Publishing Co. 1964.
16. SHERWOOD, R. C., REMEIK, J. P., WILLIAMS, H. J.: *J. Appl. Phys.* **30**, 217 (1959).
17. WILLIAMS, H. J., SHERWOOD, R. C., REMEIK, J. P.: *J. Appl. Phys.* **29**, 1772 (1958).
18. ABRAHAM, S. C.: *Mat. Res. Bull.* **6**, 881 (1971).
19. KLASSEN-NEKLYDOVA, M. A.: *Mechanical twinning of crystals*. New York: Consultants Bureau 1964.
20. ROGERS, A. F., KERR, P. K.: *Optical mineralogy*. New York: McGraw-Hill Book Co. 1942.
21. BRAGG, W. L.: *Atomic structure of minerals*. Ithaca, N. Y.: Cornell University Press 1937.
22. MÜGGE, O., HEIDE, F.: *Neues j.b. Mineral. Abt. A* **64**, 163 (1931).
23. LAVES, F.: *Naturwissenschaften* **39**, 546 (1952).
24. STARKEY, J.: *Schweiz. Mineral. Petrogr. Mitt.* **47**, 257 (1967).
25. AXE, J. D.: *Trans. Am. Cryst. Assoc.* **7**, 89 (1971).
26. SAIFI, M. A., CROSS, L. E.: *Phys. Rev. B* **2**, 677 (1970).
27. ROTH, W. L.: *J. Appl. Phys.* **31**, 2000 (1960).
28. SLACK, G. A.: *J. Appl. Phys.* **31**, 1571 (1960).
29. THOMAS, L. A., WOOSTER, W. A.: *Proc. Roy. Soc. (Lond.) A* **208**, 43 (1951).
30. LEVY, H. A., PETERSON, S. W.: *Phys. Rev.* **86**, 766 (1952).
31. GOLDSCHMIDT, G. H., HURST, D. G.: *Phys. Rev.* **83**, 88 (1951).
32. MOHLER, E., PITKA, R.: *Solid State Commun.* **14**, 791 (1974).
33. BAHR, S., ENGL, J.: *Z. Phys.* **105**, 470 (1937).
34. PICKART, S. J.: *Bull. Am. Phys. Soc.* **5**, 357 (1960).
35. BOROVIK-ROMANOV, A. S., ALEKSANJAN, G. G., RUDASHEVSKII, E. G.: *Int. Conf. on Magnetism and Crystallography*. Kyoto, Japan, Paper 155, 1962.
36. LANDAU, L. D., LIFSHITZ, E. M.: *Electrodynamics of continuous media*. Reading, Mass.: Addison-Wesley Publishing Co. 1960.
37. BERTAUT, E. F., MERCIER, M.: *Mat. Res. Bull.* **6**, 907 (1971).
38. SANTORO, R. P., NEWNHAM, R. E.: *Acta Cryst.* **22**, 344 (1967).
39. BOZORTH, R. M., KRAMER, V.: *J. Phys. Radium* **20**, 393 (1959).
40. SHTRIKMAN, S., TREVES, D.: *Phys. Rev.* **130**, 986 (1963).
41. BRIKNER, L. H., BIERSTEDT, P. E., JAEP, W. F., BARKLEY, J. R.: *Mat. Res. Bull.* **8**, 497 (1973).
42. NEWNHAM, R. E., CROSS, L. E.: *Mat. Res. Bull.* **9**, 927, 1021 (1974).

V. Optical Materials

The refractive index for transparent materials is equal to the ratio of the speed of light in vacuum to that in the material. Because of their low densities, gases have refractive indices near 1, while for liquids and solids n ranges between 1.3 and 3. The magnitude of n is determined chiefly by density of packing and the polarizability of the ions. Densely packed arrays of highly polarizable groups result in large refractive indices.

Refractive index depends on wavelength, giving rise to dispersion. For most transparent substances, n increases as λ decreases; refractive indices for violet light are generally a few percent larger than those for red. Dispersion is caused by electronic transitions in the ultraviolet region. When the photon energy approaches the value required for transition, the electrons undergo wide excursions, producing large polarizability and large refractive indices.

Many of the new devices proposed for optical communication systems require transparent materials with large refractive indices. This means that materials with transitions in the near ultraviolet are of special interest. The index of refraction is inversely related to the band gap E_g . WEMPLE and DIDOMENICO [1] have shown that for oxides the relation approximates

$$n^2 \cong 1 + \frac{15}{E_g},$$

where E_g is expressed in electron-volts. Other classes of materials may have somewhat different constants. If an oxide is to be transparent throughout the visible range, the equation states that the band gap must be at least $hc/4000 \text{ Å} \cong 3 \text{ eV}$, giving $n \cong 2.5$. To obtain higher refractive indices, the minimum wavelength must be raised, closing the window. The shortest wavelength for which transmission is desired determines the maximum refractive index.

The empirical Gladstone-Dale relation is useful in predicting refractive indices,

$$n = 1 + \rho \sum_i p_i k_i,$$

where ρ is density, and p_i and k_i are the weight fraction and refractive coefficient of the i th component. An abbreviated table of refractive co-

Table 13. Refractive coefficients for some common oxide constituents for use in the Gladstone-Dale relation. After LARSEN and BERMAN [2]

	Molecular weight	k		Molecular weight	k
H ₂ O	18	0.34	Y ₂ O ₃	226	0.14
Li ₂ O	30	0.31	La ₂ O ₃	326	0.15
Na ₂ O	62	0.18	Bi ₂ O ₃	464	0.16
K ₂ O	94	0.19	CO ₂	44	0.22
BeO	25	0.24	SiO ₂	60	0.21
MgO	40	0.20	TiO ₂	80	0.40
CaO	56	0.23	ZrO ₂	123	0.20
SrO	104	0.14	SnO ₂	151	0.15
BaO	153	0.13	N ₂ O ₅	108	0.24
PbO	223	0.15	P ₂ O ₅	142	0.19
B ₂ O ₃	70	0.22	Nb ₂ O ₅	268	0.30
Al ₂ O ₃	102	0.20	SO ₃	80	0.18

efficients is given in Table 13. To illustrate its use we calculate the predicted refractive index for pyrope garnet, Mg₃Al₂Si₃O₁₂. The molecular weight is 402 and the specific gravity 3.56. The constituent oxides are 3MgO + Al₂O₃ + 3SiO₂, for which the weight fractions are $3 \times 40/402$, $102/402$, and $3 \times 60/402$. Substituting in the Gladstone-Dale formula using the k values in Table 13 gives $n = 1 + 3.56 (0.3 \times 0.20 + 0.253 \times 0.20 + 0.447 \times 0.21) = 1.71$, in good agreement with the observed value 1.72. The equation gives agreement to within 5% for a wide range of oxides. It works well because of the additivity of atomic polarizabilities which change little from compound to compound.

A few of the constituent oxides in Table 13 possess unusually large refractive coefficients. The k value for TiO₂ is twice that of most others, for instance. This is one of the oxides with electronic transitions in the very near ultraviolet, a transition from the 2p level of O²⁻ to the 3d orbital of Ti⁴⁺. The presence of this low-lying excited state augments the electronic polarizability which in turn contributes to the refractive index, the dielectric constant, and to ferroelectricity in a number of titanates.

The development of a low-loss optical transmission line is crucial to the implementation of a laser communication system. In a glass-fiber optical waveguide the light beam is confined within and guided along a solid glass fiber of circular cross-section. The fibers are less than a millimeter in diameter, and can be arranged in bundles and strung like cables.

Self-focusing fibers have been developed by controlling the refractive index. By making the refractive index at the center of the fiber larger

than at the surface, a light beam injected at one end of the fiber is guided along by total internal reflection. The desired refractive index profile can be achieved by ion-exchange techniques in which, for example, thallium ions in the glass are replaced by sodium ions with smaller polarizability. Ions near the surface will be replaced more rapidly than the center, giving a composition gradient and a refractive index gradient. This results in a high-index core surrounded by a low-index sheath, causing light beams to be focused in the center.

For long distance communications systems, it is essential that signal losses be kept at low levels, below 20 dB/km. Bulk scattering losses caused by inhomogeneities in the glass are important at short wavelengths. Vibration losses dominate in the infrared, and transition-metal impurities in the visible range [3]. Impurity absorption arises principally from iron, cobalt and chromium. Concentrations below a few parts per billion are necessary if absorption below 20 dB/km is to be attained. Hydroxyl ions are another important impurity since the third and fourth harmonics of the O-H stretching frequency occur at 9500 and 7250 Å.

1. Luster

Refractive index determines the intensity of reflected light from a surface. The luster of a solid refers to its appearance in reflected light. For normal incidence on a smooth surface, the ratio of reflected intensity to incident intensity is

$$R = \frac{(n-1)^2 + n^2 k^2}{(n+1)^2 + n^2 k^2}$$

The refractive index is n and k the absorption index. For transparent materials, $k=0$ and R depends on n only. Only about 2% of the light is reflected for low-index solids, giving them a glassy-like appearance. The high reflectivity of diamond ($n=2.41$, $R=17\%$) imparts a high luster to the stone.

The luster of various solids are compared in Table 14. Most ionic solids have low refractive indices and vitreous luster. Extended covalent bonding leads to larger refractive indices and adamantine luster. The large absorption coefficients of metals results in very high reflectivities.

Not all solids have smooth surfaces. The diffuse scattering caused by surface roughness gives a *dull* luster, as in clay bodies. Incipient cleavage and surface films can produce an *iridescent* luster because of interference effects. Satin spar, a fibrous variety of gypsum, shows a *silky* luster.

Table 14. Reflection coefficients for several types of luster, together with mineral examples [4]

	R	Example
Transparent crystals		
Subvitreous	< 4%	fluorite, CaF_2
Vitreous	4–8%	topaz, $\text{Al}_2\text{SiO}_4\text{F}_2$
Subadamantine	8–14%	zircon, ZrSiO_4
Adamantine	14–21%	diamond, C
Adamantine Splendent	> 21%	cinnabar, HgS
Opaque crystals		
Submetallic	< 20%	ilmenite, FeTiO_3
Metallic	20–50%	molybdenite, MoS_2
Metallic Splendent	> 50%	gold, Au

2. Birefringence and Crystal Structure

The optical properties of crystals can be visualized using the indicatrix, an ellipsoid showing the variation of the refractive indices with vibration direction. Each radius vector from the center to the surface represents a vibration direction whose length measures the index of refraction of a wave vibrating parallel to the radius vector.

Like all geometric representation of physical properties, the indicatrix must include the symmetry elements of the point group (Neumann's Law). The ellipsoid of revolution and the sphere are special cases of a general ellipsoid in which two or all three of the principal axes are equivalent. The point symmetry of a general ellipsoid is $\frac{2}{m} \frac{2}{m} \frac{2}{m}$ (mmm is shortened form) with 2-fold axes parallel to the three principal axes. All crystallographic point groups belonging to the orthorhombic, monoclinic, and triclinic systems are subgroups of mmm , and therefore the optical properties can be represented by a general ellipsoid. The orientation of the indicatrix is constrained by symmetry in orthorhombic and monoclinic crystals. For orthorhombic crystals the principal axes are parallel to the crystallographic axes, the three two-fold axes. There is only one two-fold axis in monoclinic point groups so that the indicatrix is only partially constrained with one major axis parallel to the 2-fold axis, b .

A general ellipsoid does not possess rotational symmetry higher than 2. Therefore, trigonal crystals, with a three-fold axis parallel to c , place further constraints on the indicatrix. The indicatrix for trigonal crystals is an ellipsoid of revolution with the circular section per-

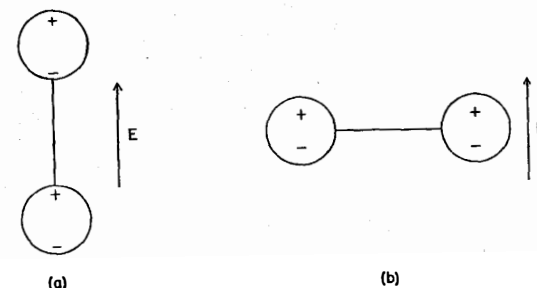


Fig. 48 a and b. Diatomic molecules in an electric field

pendicular to c . A circle contains three-fold symmetry but an ellipse does not. The same argument holds for tetragonal and hexagonal crystals.

Cubic crystals contain four three-fold axes, converting the ellipsoid to a sphere. The refractive index is then identical for all vibration directions making cubic materials optically isotropic.

In transparent materials, refractive index is proportional to the square root of the electronic polarization. The latter is in turn proportional to the polarizabilities of the ions in the crystal and also to the local electric field. Calculations on calcite and aragonite by W. L. BRAGG [5] show how birefringence is related to structure.

To illustrate, consider the diatomic molecule in Fig. 48. In (a) the electric vector of the light wave is parallel to the length of the molecule and in (b) it is perpendicular. The electric dipole moment of the atom is equal to the product of the local field and the polarizability. The local field is the vector sum of the applied field E and dipole field associated with the neighboring atom. In the parallel orientation (a) the dipole field of the neighboring atom enhances E so that both atoms are polarized more, giving rise to larger dipole moments and a larger refractive index for this polarization direction. The opposite effect occurs in (b). Here the dipole field is in opposition to E , reducing the dipole moments and refractive index. Thus waves polarized parallel to the molecule travel slower than waves polarized perpendicular to the molecule, creating birefringence in crystals with aligned molecules.

Birefringence in many compounds containing molecular groups can be explained in this way. Some examples are given in Table 15. When molecular groups are parallel to one another, the optical indicatrix mimics the molecular shape. The flat CO_3^{2-} groups in calcite oriented give rise to an indicatrix flattened perpendicular to c .

When flat molecules are parallel to one another, a large negative birefringence results with the vibration direction of lowest index per-

Table 15. Optical constants of crystals with parallel aspherical radicals or molecules

	Molecular shape	α	β	γ	Optic sign
$\text{Ca}(\text{OCl})_2 \cdot 3\text{H}_2\text{O}$	Linear molecule	1.535	1.535	1.63	+
NaNO_2	Obtuse V-shaped	1.340	1.425	1.655	+
KClO_3	Low pyramid	1.410	1.517	1.524	-
C_{10}H_8	Flat with parallel planes	1.422	1.775	1.932	-

pendicular to the plane of the molecules, as in naphthalene. When the planar molecular groups are not parallel to one another but are parallel to a common direction, positive birefringence results with the vibration direction of large refractive index along the common direction. An example is vaterite, μCaCO_3 .

For linear or near-linear groups, positive birefringence occurs when they are parallel to another and negative when they are not parallel but lie in a common plane perpendicular to a common direction.

Refractive indices are closely related to optical band gap E_g because of dispersion, and both can often be correlated with structural variations. The ZnS and SiC polytypes are good examples [6, 7]. These structures are intermediate between the cubic sphalerite structure and the hexagonal wurtzite structure, so that the various polytypes can be characterized by parameter α which refers to fraction of layers stacked in hexagonal

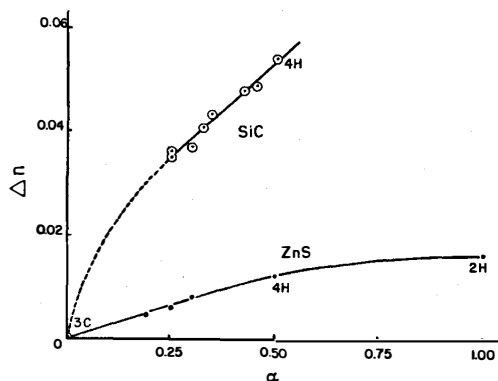


Fig. 49. Birefringence Δn plotted against hexagonality α for several ZnS and SiC polytypes [6, 7]. Birefringence decreases as the fraction of cubic close packed layers increases because cubic crystals are optically isotropic

closepacked order. Thus $\alpha = 0$ for the 3C polytype sphalerite and $\alpha = 1$ for wurtzite with all other polytypes in between 0 and 1.

Several of the physical properties of these compounds can be correlated with α , including absorption edges, color, and birefringence (Fig. 49). As might be expected the birefringence disappears as α approaches zero since the structures are becoming more cubic.

3. Optical Windows

Prisms, lenses, windows, and other optical components require materials which are transparent over wide wavelength ranges. The range of greatest interest spans the visible and near infrared spectrum, and is bounded on the short wavelength size by the electronic band gap: $\lambda_{\min} = hc/E_g$, where h is Planck's constant, c the speed of light in vacuum, and E_g the band gap energy. At the other end, infrared-active lattice vibrations determine the maximum wavelength transmitted. The weak bands observed between these two limits generally involve impurities and are therefore subject to control.

To broaden the window as much as possible, it is desirable to have a very high energy band gap and very low energy vibration modes. Only diamond comes close to satisfying these conditions. It has a wide band gap (6 eV) and no active infrared modes, but is rather expensive. Silicon and germanium are also excellent infrared windows but do not transmit visible radiation because of their narrow band gaps. Most of the other chemical elements are either metals or gases, and are therefore unsuitable as windows.

All compounds possess local dipole moments and infrared-active vibration modes. Stretching modes, in which neighboring cations and anions vibrate out of phase with one another, generally limit the infrared window. Strongly bonded ions of low coordination number are usually involved in the highest frequency infrared mode. Thus in a magnesium silicate, for example, the Si-O absorption bands are lower frequency than are the Mg-O bands. It is unfortunate that the strongest bonded materials also have the highest energy infrared modes, for it is those which have the widest band gaps.

Polyatomic inorganic ions exhibit characteristic infrared spectra which are useful in chemical identification and in structure analysis. Strongly-bonded triangular groups (CO_3^{2-} , BO_3^{3-} , NO_3^-) show an intense absorption band near 7μ . The tetrahedral ions SiO_4^{4-} , PO_4^{3-} , SO_4^{2-} , ClO_4^- absorb between 9 and 10μ and pyramidal groups such as ClO_3^- , BrO_3^- and IO_3^- possess a band at slightly longer wavelengths in the $10\text{--}13\mu$ range. These are the principal bands but each group shows a number of

Table 16. Infrared window materials [8]

IRTRAN	Composition	Transmission range
1	MgF ₂	0.4– 9 μ
2	ZnS	0.3–15 μ
3	CaF ₂	0.2–12 μ
4	ZnSe	0.5–22 μ
5	MgO	0.2– 9 μ
6	CdTe	0.8–32 μ

weaker spectra which make identification conclusive. Hydrogen bond stretching vibrations lie near 3 μ .

Atomic mass is important as well as bond strength. Heavy atoms have lower resonant frequencies than do light ones. Thus O–H vibrations are very high frequency although the bonding is not particularly strong. For the same reason, heavy alkali halides such as TlI are used in making infrared windows. In summary, far-infrared transmission requires compounds with large masses and weak bonding (low force constants and high coordination numbers). The mechanical properties of such crystals tend to be poor.

Durable infrared materials have been developed for missile domes and numerous military and industrial infrared applications. The Kodak IRTRAN series are typical of the polycrystalline infrared windows manufactured by hot-pressing methods. These materials are mechanically strong and chemically and thermally stable over wide environmental conditions. Transmission ranges for the IRTRAN materials (Table 16) show the superiority for compounds with high atomic numbers, making materials such as cadmium telluride useful as infrared windows. The disadvantages are large reflection losses associated with high refractive indices, poor short-wavelength transmission, caused by a narrow band gap, and mechanical softness.

Many inorganic crystals become highly reflecting at certain characteristic wavelengths in the infrared. The reflectivities approach those of metals but are confined to narrow characteristic regions related to the principal infrared absorption bands. Because of these bands, certain alkali halide crystals make excellent selective reflectors. Infrared wavelengths corresponding to the regions of high reflectivity can be isolated from a continuous source by successive reflections from several crystal surfaces. The near-monochromatic reflected beams are called residual rays, or restrahlen. Crystals containing elements of low atomic weight have low wavelength restrahlen. Residual-ray wavelengths for several

alkali halides are as follows: LiF 20 μ , NaCl 52 μ , KCl 63 μ , KBr 82 μ . The restrahlen of thallium bromiodide (KRS-5) is in the far infrared at 120 μ . KRS-5 has the CsCl structure, while most of the other alkali halides have the rocksalt structure (Fig. 50).

Extensive research programs have been initiated to obtain materials suitable for high-power infrared systems. Window materials are needed for CO₂ lasers operating at 10.6 μ m, and for chemical lasers operating in the 2–6 μ m range. Some materials with high absorption at 10.6 μ m are

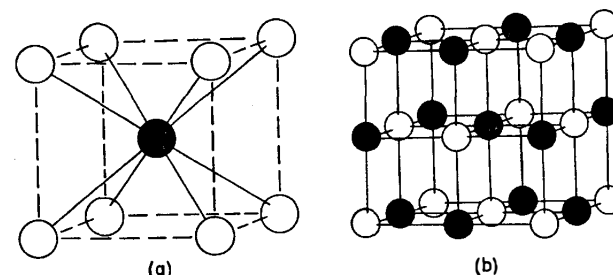


Fig. 50a and b. The cesium chloride (CsCl) (a) and rocksalt (NaCl) (b) structures

sufficiently transparent for use in the 2–6 μ m range. This is important because window materials for the very near IR such as Si, Ge, and the alkaline earth fluorides, have better mechanical and thermal properties than do KBr, KCl, and other 10.6 μ m materials.

The total power that a window can transmit under specified conditions has been used as a figure of merit [9]. Optical distortion caused by changes in thickness and refractive index with temperature is an important consideration. For alkaline-earth fluorides the effects of thermal expansion and temperature dependence of the refractive index nearly cancel one another, with the result that the optical distortion is less than that for other materials. The allowable temperature gradient for a 10 cm BaF₂ window is 50 °K, compared to about 1 °K for most other 4 μ m window materials. In the case of small (1 cm) windows, radial heat flow is more important since edge-cooling becomes practicable. Under these circumstances, silicon has a large figure of merit because of its large thermal conductivity.

4. Color

The attractive colors of gemstones and other colored inorganic solids are usually due to absorption bands in the visible spectrum, though diffraction effects are occasionally important, as in opal. The visible

Table 17. The spectral colors, their wavelengths and complementary colors

λ (Å)	Spectral color	Complementary color
4100	violet	lemon-yellow
4300	indigo	yellow
4800	blue	orange
5000	blue-green	red
5300	green	purple
5600	lemon-yellow	violet
5800	yellow	indigo
6100	orange	blue
6800	red	blue-green

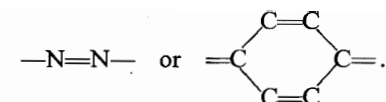
spectrum extends from 4000 to 7000 Å; in this region electronic transitions are the most important. There are four common types: 1. internal transitions within transition-metal, rare-earth, or other ions with incomplete electron shells, 2. charge transfer processes in which an electron is transferred from one ion to another, 3. electronic transitions associated with crystal imperfections, and 4. band gap transitions—intrinsic coloration found in many semiconductor compounds. Types (1)–(3) are usually associated with small amounts of impurities or defects, whereas (4) is a bulk property.

The following examples will serve to illustrate the various types and the cause of color in crystals. The spectral colors and their wavelengths are given in Table 17. When an absorption band removes a certain color from the transmitted beam, the eye collects the remaining colors, “seeing” the complementary color to the one removed. Thus when red light is absorbed—as by Fe^{2+} in olivine—the crystal appears green, the complementary color. In oxides and fluorides containing transition-metal ions, the absorption bands and color depend principally on the nature of the ion and secondarily on the strength and symmetry of the crystal field. The electron configuration of the ion is most important. Thus Fe^{3+} with five 3d electrons and a relatively stable half-filled shell, has a far different spectrum than that of Fe^{2+} . Chrysoberyl $(\text{Al}, \text{Fe}^{3+})_2\text{-BeO}_4$ has almost the same structure as olivine $(\text{Mg}, \text{Fe}^{2+})_2\text{SiO}_4$ yet the spectra are vastly different. Trivalent iron absorbs in the violet region, giving chrysoberyl a pale yellow complementary color [10].

Some crystals absorb light differently for different polarization directions. The effect is called pleochroism in biaxial crystals and dichroism in uniaxial crystals. Cubic crystals do not show differential light absorption under normal circumstances. In a few minerals such as cordierite, pleochroism is apparent even in unpolarized light. Tourmaline

(class 3m) absorbs light strongly for vibration directions perpendicular to the trigonal axis but only weakly when the electric vector is parallel to *c*. For many years mineralogists used tourmaline “tongs” made of crossed tourmaline crystals to examine minerals in polarized light. The dichroism of tourmaline arises from $\text{Fe}^{2+}(t^4e^2)$ to $\text{Fe}^{3+}(t^3e^2)$ charge transfer transitions [11]. Di- and trivalent iron occupy octahedral sites in tourmaline with the octahedra clustered in brucite-like arrangements separated by borosilicate groups. The octahedra share edges in planes parallel to (0001) so that when the electric vector of the light wave is perpendicular to *c*, the electrons move between octahedra, hopping from one cation to the next, and absorbing light.

In organic dichroic materials, internal absorption takes place when the electric polarization vector is parallel to the direction of chromophoric groups, along chemical linkages such as



If such groups are arranged parallel to one another in the crystal, strong pleochroism results.

Crystal fields are important in determining the colors of transition-metal compounds because the incomplete 3d shell is near the outside of the ion. The colors of rare-earth ions, on the other hand, are insensitive to structure because the 4f shell is buried deep in the atom. Transition metal ions are usually found in tetrahedral or octahedral coordination in oxides and fluorides. The two coordinations usually show different spectra and different colors because the electronic ground state is often different for tetrahedral and octahedral fields. Co^{2+} , for example, has a $e^4t_2^3$ ground state in tetrahedral environment and $t_{2g}^5e_g^2$ symmetry in an octahedral field. Not only the symmetry of the field is important, but its strength as well. Chromium bearing oxides illustrate this point: chromia, emerald, and most chromium containing oxides are green, but ruby, spinel and a few others are red. Alexandrite is red or green, depending on the source of illumination. The intense absorption bands of Cr^{3+} shift towards higher energy for the larger crystal fields (Fig. 51). Large crystal fields are caused by close neighbors. In ruby the Cr–O distances are about 0.1 Å shorter than in Cr_2O_3 , and as a result, the important ${}^4\text{A}_2 \rightarrow {}^4\text{T}_1$ and ${}^4\text{A}_2 \rightarrow {}^4\text{T}_2$ absorption bands shift about 400 Å, changing the color from red to green.

Colors are also associated with imperfections in solids. When colorless alkali halide crystals are irradiated or heated in the alkali vapor they change color: NaCl becomes yellow, KBr blue, and KCl magenta.

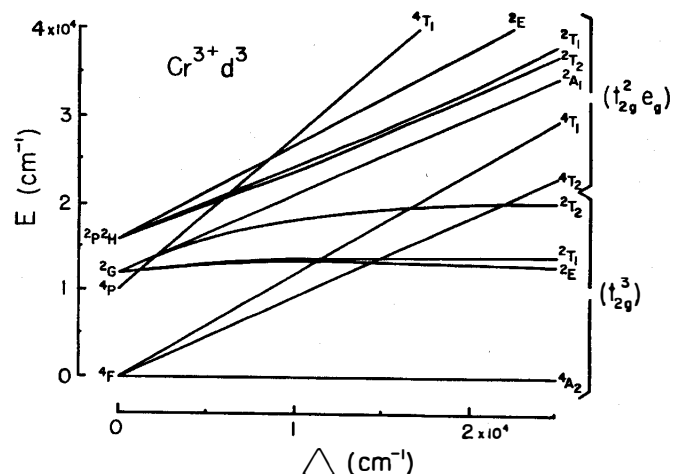


Fig. 51. Energy-level diagrams for octahedrally coordinated Cr^{3+} plotted as a function of the crystal-field parameter Δ

The most common type of coloring imperfection is the F-center (Farbzentrum) in which single electrons are trapped in anion vacancies. Visible radiation is absorbed by the trapped electron whose energy states can be approximated by hydrogen-like wave functions.

Undoped semiconductor crystals are colored according to the band gap. Si and Ge are metallic-looking because all visible radiation promotes electrons to the conduction band. CdS ($E_g = 2.45 \text{ eV}$) is yellow because blue and violet light can promote electrons but the longer wavelengths cannot. Hence blues are absorbed and the crystal appears yellow, the complementary color.

5. Crystalline Lasers

Laser action has been obtained in crystals, glasses, gases, semiconductors and liquids, at resonant frequencies ranging from the far infrared to the ultraviolet. Only oxide and semiconductor lasers will be discussed here, though other types are widely used. Among the advantages of doped-oxide lasers are long-lifetime excited states, high thermal conductivity, and high melting points, all of which are useful in the generation of high peak powers. In addition, some systems show narrow fluorescence linewidths and are therefore of interest as frequency standards.

Two of the most popular high-power lasers are ruby and neodymium-doped YAG, yttrium aluminum garnet [12]. In the ruby laser, the first to be discovered, the Al_2O_3 host lattice is doped with about 0.05% Cr. Three electronic transitions within the chromium d -shell are used to obtain the laser beam. Light absorbed from the pump source (usually a flash lamp), raises Cr^{3+} from the ${}^4\text{A}_2$ ground state to one of the ${}^4\text{T}$ states associated with broad absorption bands in the visible (Fig. 51). From there the atoms decay rapidly to the narrow ${}^2\text{E}$ states by phonon emission. Population inversion is achieved when more Cr atoms are in the excited ${}^2\text{E}$ level than the ${}^4\text{A}_2$ ground state. Stimulated emission then leads to light amplification at wavelengths near 6930 \AA .

Yttrium aluminum garnet doped with 1% Nd is usually operated as a four-level laser. After being pumped from the ${}^4\text{I}_{9/2}$ ground state to one of the higher excited states, the neodymium ions decay to the long-lived ${}^4\text{F}_{3/2}$ state. The 1.06μ laser transition is between ${}^4\text{F}_{3/2}$ and ${}^4\text{I}_{11/2}$, another excited state of lower energy. Four-level lasers have lower threshold energies than three-level systems because the terminal state is not thermally populated, making population inversion easier to achieve.

The selection of laser materials evolves on the choices for host lattice and dopant. Since laser action takes place between the electronic states of a single shell, the $3d$ transition series and the $4f$ rare earth series are logical choices. The $4f$ electrons of the rare earth ions are relatively close to the nucleus, interacting little with the surroundings. As a result, electronic transitions within the $4f$ shell yield sharp line spectra similar to those of the free ion. Such narrow linewidths are helpful in achieving low thresholds, but broader absorption bands are needed for efficient pumping. To obtain sufficient absorption, high doping levels are required for trivalent rare earth ions.

Chromium is the best of the transition metal ions, though Ni^{2+} and Co^{2+} doped fluorides have been operated as low-temperature infrared lasers. The combination of broad absorption bands and narrow emission lines for Cr^{3+} make it nearly ideal (Fig. 51).

Various doping combinations have been suggested in attempting to improve the overall efficiency. In one such system $\text{Y}_3\text{Al}_5\text{O}_{12}$ is doped with both Cr^{3+} and Nd^{3+} . Pumping light is absorbed by the Cr^{3+} ions which transfer excitation energy to Nd^{3+} , which produces laser action in returning to its ground state. The processes governing cross transfer are not well understood, but sensitized systems such as this appear to work well in the infrared where competing spontaneous emission rates decrease.

The host lattice must of course accommodate the active impurity ions. Trivalent chromium prefers octahedral sites, while the larger rare earth ions are often found in eight coordination. The host lattice creates

a crystal field which removes the degeneracy of the free ion states and is a major factor in determining electronic energy levels, especially for transition metal ions. The site symmetry also effects selection rules. Low symmetry promotes orbital mixing, making transitions easier. High-power pulsed lasers (Q-switching) require long lifetimes because of the time delay between pulses. Cubic site symmetries such as those in $\text{LaAlO}_3:\text{Cr}^{3+}$ are good candidates for such applications.

6. Semiconductor Lamps

Light emission from semiconductor junctions has been studied for twenty years, but only recently have commercial products begun to appear. The difficulties in construction can be traced to three design criteria. First, the light emission must be in the visible range, 4500–6800 Å. Second, it must be possible to make $p-n$ junctions in the base semiconductor material. Third, the conversion of electrical energy to visible light must be relatively efficient. Luminous efficiencies of 0.1 to 0.2 lumens/W are required for light-emitting diodes. Based on two recent developments, it now appears possible to satisfy these criteria [13].

Substantial advances have occurred in the preparation of III-V semiconductor compounds, most notably $\text{GaAs}_{1-x}\text{P}_x$ and $\text{In}_{1-x}\text{Ga}_x\text{P}$. These solid solutions crystallize in the cubic zincblende structure (Fig. 12). By adjusting the composition of the ternary alloy, the energy-bands are altered to adjust the color of the emitted light.

The second important development is the recognition of the role of isoelectronic impurities, especially nitrogen. Isoelectronic impurities improve the efficiency of high-frequency light emission in $\text{GaAs}_{1-x}\text{P}_x$ and $\text{In}_{1-x}\text{Ga}_x\text{P}$ diodes. Nitrogen substitutes for arsenic or phosphorus in the zincblende structure but behaves somewhat differently. A short-range electronic potential is developed which leads to the binding of an electron with energies of about 10–100 meV, depending on doping levels. Electronic states are broadened by the interaction of N-N pairs and by the variations in local fields found in a ternary alloy. The short range of this potential compared to the long range coulomb potential of charged impurities is important in breaking the momentum conservation selection rule in optical absorption and emission. As a result of the N-traps, $\text{GaAs}_{1-x}\text{P}_x$ and other crystals with indirect band gap transitions become more efficient in the conversion of electric current to light. Light emitting diodes are now being used in countless read-out and display applications including small calculators, instrument panels, and household appliances. A continuous range of colors from red through green has been made possible by the substitution of nitrogen in ternary III-V alloys.

7. Luminescence

Inorganic phosphors are used in fluorescent lamps and television screens. Solid state displays utilizing electroluminescent phosphors and light-emitting diodes are also under development, though such lighting schemes are too inefficient for many applications.

The phosphorescent materials used in fluorescent lamps convert the 1850 and 2540 Å radiation of a mercury arc into visible light. Thousands of combinations of activator ions and host crystals have been studied to produce efficient light conversion. Phosphors can be grouped into three major classes based on the electronic state of the activator center.

In *primary activators* the electron configuration of emitting excited state differs in parity from the electron configuration of the ground state. Examples include Sn^{2+} , Pb^{2+} , Sb^{3+} , Cu^+ , Ce^{3+} , and Eu^{2+} . In Sb^{3+} the ground state is $4d^{10}5s^2$ and the emitting state is $4d^{10}5s5p$. In Cu^+ and Eu^{2+} phosphors, fluorescence occurs via $3d^94p \rightarrow 3d^{10}$ and $4f^65d \rightarrow 4f^7$ transitions, respectively. A common characteristic of activators in this class is the rapid decay of fluorescence, typically microsecond or less. In using primary activators about 1–10 percent of the host cations are replaced by activator ions.

Electronic configurations of the ground state and emitting state are identical in parity in *secondary activators*. In divalent manganese, for example, fluorescence takes place between $3d^5$ states. Other activators in this class include Cr^{3+} , Mn^{4+} , Sm^{3+} , and Tb^{3+} . Secondary activators have a rather slow rate of decay with half-lives in the millisecond range. Concentrations used in practical phosphors are about 0.5–5%. To excite such phosphors it is generally necessary to make use of energy transfer from an excited complex ion, although the secondary activators can be excited directly by ultraviolet light if configuration changes can be induced. Wavelengths shorter than 200 nm are sufficiently energetic to excite Mn^{2+} to its $3d^44p$ states.

The third class of phosphors are activated by *complex ions* as in the tungstates where the W^{6+} ion has a $5p^6$ ground state configuration. Other central ions of interest are Mo^{6+} , Nb^{5+} , Ta^{5+} , V^{5+} , and Ti^{4+} , all with filled p shells. This class of phosphors is characterized by microsecond decay times and broad emission bands. There is also evidence that d^{10} ions such as Zn^{2+} and Cd^{2+} are also effective complex ion phosphors. A number of cadmium and zinc compounds are effective host lattices for Mn^{2+} .

To illustrate the importance of crystal chemistry in phosphor development, consider photoluminescence in oxide phosphors. The classic example is willemite, Zn_2SiO_4 , activated with about 1% Mn^{2+}

replacing zinc. Other commonly used fluorescent centers, ions with metastable excited states, are Cu^+ , Bi^{3+} , Sn^{2+} , Cr^{3+} , Ce^{3+} , and Eu^{3+} . Killer ions like Fe^{2+} , Ni^{2+} , and Co^{2+} with radiationless transitions to the ground state can ruin luminescence and must be excluded in preparing phosphors.

Photoluminescence is a three-step process: 1. absorption of an ultra-violet photon, 2. transfer of the excitation energy to the fluorescent center, and 3. radiative emission by the fluorescent center. The second step is unimportant in phosphors with direct excitation, as in Eu^{3+} activated Y_2O_3 illuminated with wavelengths greater than 2700 Å. In this case Eu^{3+} acts as both absorber and emitter. Indirect excitation takes place in $\text{YVO}_4:\text{Eu}^{3+}$ where the vanadate group absorbs and Eu emits. An efficient transfer process is needed in this case. Energy transfer may take place *via* three mechanisms: 1. charge carriers, 2. radiative emission and absorption, or 3. non-radiative processes such as multipole or exchange mechanisms. Charge transfer appears to dominate in $\text{YVO}_4:\text{Bi}^{3+}$ phosphors while superexchange occurs in a number of Eu^{3+} activated phosphors. The V–O–Eu angle is important in energy transfer; in $\text{YVO}_4:\text{Eu}^{3+}$ the angle is about 170° giving rapid transfer of energy and high photoluminescence efficiency. The angle is 50° smaller in the Eu activated garnet $\text{NaCa}_2\text{Mg}_2\text{V}_3\text{O}_{12}$ which has a low efficiency. Similar results were obtained in other phosphors [14].

Crystal structure is not only important in the energy transfer process but in absorption and emission as well. Atomic levels are modified by crystal fields which can drastically change the intensity and wavelength distribution of the emitted radiation. Electronic energy levels for Cr-activated phosphors are shown in Fig. 51. The splitting between the ^4T excited state and the ^4A ground state is determined by the crystal field parameter Δ . The ^2E – ^4A splitting is nearly independent of Δ . Hence, the relative position of the two excited states is controlled by the crystal field. In ruby ($\text{Al}_2\text{O}_3:\text{Cr}$), the crystal field is large so that emission occurs from ^2E to ^4A , giving sharp line fluorescence. Broad band emission from ^4T to ^4A occurs in certain Cr^{3+} activated niobates and tungstates which have weaker crystal fields. Wavelengths and colors can be altered in this way.

A third way in which crystal chemistry is important is through symmetry. When activator ions occupy high symmetry sites the excited states tend to have longer half-lives because certain selection rule violations depend on symmetry. For example, the absence of a center of symmetry promotes orbital mixing with a detrimental effect on excitation half-life. This is important for persistent phosphors.

Synthetic fluorapatite is used as a phosphor in fluorescent lamps, activating $\text{Ca}_5(\text{PO}_4)_3\text{F}$ with Mn and Sb. Divalent manganese fluoresces

red and trivalent Sb blue. Both are broad band emitters so that adjusting the proportions of the two activators gives white light. The color rendition is further controlled by substituting small amounts for Cl for F in the host lattice apatite. The substitution "tunes" the crystal field about the calcium sites, shifting the energy levels and changing the emission wavelengths.

Two factors governing the usefulness of a phosphor are color and quantum efficiency. Consider first the influence of crystal structure on the excitation and emission transitions. Eu^{3+} phosphors are of great practical importance as red phosphors for color television screens. Intense luminescence in europium compounds is caused by electronic transitions from the $^5\text{D}_0$ excited state to $^7\text{F}_1$ or $^7\text{F}_2$. The $^5\text{D}_0 \rightarrow ^7\text{F}_1$ emission is orange (0.59μ), while $^5\text{D}_0 \rightarrow ^7\text{F}_2$ is red (0.61μ). The wavelengths are little affected by local fields, since $4f$ electrons are well shielded.

The environment does, however, affect selection rules strongly. Parity prohibition can be lifted only by the influence of the crystal lattice. If the rare earth ion is located at a center of symmetry, then odd crystal field terms are absent, and only magnetic-dipole transitions are possible, favoring the $^5\text{D}_0 \rightarrow ^7\text{F}_1$ transition in Eu^{3+} . In europium-doped host lattices such as $\text{Ba}_2\text{GdNbO}_6$, NaLuO_2 , and $\text{Gd}_2\text{Ti}_2\text{O}_7$, Eu^{3+} occupies an inversion center. The emission is orange in all three compounds. More intense electric-dipole transitions are possible when the Eu^{3+} position is acentric. The selection rule is $\Delta J = 2, 4$, or 6 in this case, favoring the $^5\text{D}_0 \rightarrow ^7\text{F}_2$ transition. Red emission is observed from $\text{NaGdO}_2:\text{Eu}^{3+}$ and other compounds where europium is not located at a center of symmetry. The host lattice therefore controls the color of Eu^{3+} phosphors.

The quantum efficiency is the ratio of the number of photons emitted by the phosphor to the number absorbed. Phosphors of technical interest have efficiencies near 80%. To explain why certain ions luminesce and others do not, we make use of a configurational-coordinate diagram (Fig. 52). Let r be the distance between the luminescent cation and its anion neighbors. At $T = 0^\circ\text{K}$, the center occupies the lowest vibrational state of the ground state. Higher vibrational levels may be occupied when heating occurs. Excitation and emission transitions correspond to vertical transitions between the two curves. If the curves are similar in shape with Δr small, both absorption and emission lines will be narrow. Broad band spectra arise when the equilibrium distance of the excited state differs appreciably from that of the ground state. Under these conditions the separation between ground state and excited state varies with r . Rare earth spectra associated with $4f$ level transitions are generally sharp while transition-metal ions show a mixture of sharp and broad lines.

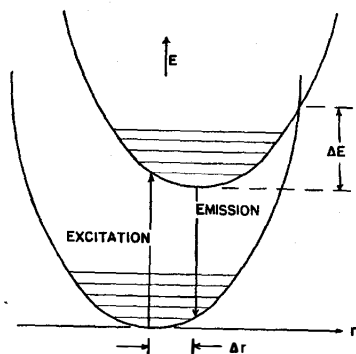


Fig. 52. The configurational diagram of a luminescent center. Potential energy curves for the ground state and excited state are plotted as a function of interatomic distance. Horizontal lines represent vibrational states. Luminescence occurs when Δr is small, ΔE is large and the temperature is low

The cross-over energy ΔE is important in luminescence. Atoms in the excited state may return to the ground state by emitting photons or phonons. The latter is referred to as a radiationless transition and predominates when ΔE is comparable to kT . Luminescence occurs when $\Delta E \gg kT$, a situation arising when Δr is small. From the configurational model, it can be seen that the equilibrium distances of the ground state and excited state must be similar to promote luminescence.

Electron orbit radii [15] provide an estimate of Δr , making it possible to predict luminescent centers. We illustrate with Mn^{2+} and Sb^{3+} , the activators used in common fluorescent lamps. For divalent manganese, emission results from electronic transitions within the $3d$ shell so that Δr is near zero. A $5p-5s$ transition occurs in Sb^{3+} . The radii for the $5p(\text{Sb})$ and $5s(\text{Sb})$ are 1.16 and 0.97 Å, respectively, giving $\Delta r = 0.19$ Å. In surveying a large number of luminescent centers, BLASSE and BRIL [16] have shown that a necessary condition for luminescence is that $\Delta r < 0.3$ Å. Not all ions satisfying this criterion are luminescent, however, because the influence of the surrounding lattice has been neglected.

The configurational diagram also shows why luminescence emission is quenched at high temperatures. When the atom is in an excited state, thermal activation may lift the energy to the intersection of the ground state and excited state. The center will then return to the equilibrium configuration of the ground state, dissipating heat in the process. Thermal quenching of the luminescence in scheelite and in $\text{Gd}_2\text{O}_3:\text{Eu}^{3+}$ occurs near 800° C. BLASSE and BRIL have developed several empirical

rules relating quenching characteristics to crystal chemistry, leading to the discovery of new high-efficiency phosphors [16].

A new class of up-conversion phosphors in which infrared radiation can be converted to visible light has received a great deal of attention in recent years [17]. These new fluorescent materials are photon excitable but differ from other phosphors in that the energy of the absorbed photons is lower than that of the emitted photons. The energy conservation principle is not violated because two or more low-energy photons are required to produce one photon of higher energy. The most practical up-conversion phosphors are doubly-doped $\text{Yb}^{3+}-\text{Er}^{3+}$ glasses and crystals in which energy transfer may take place between excited states of the two rare-earth ions. Yb^{3+} acts as the sensitizer ion which absorbs infrared radiation and transfers it to the Er^{3+} activator ion. Green luminescence is obtained when the phosphor is irradiated with near-IR photons. Two infrared photons are transferred to the Er^{3+} ion from nearby Yb^{3+} ions, raising it to a doubly excited state, and allowing emission of a visible photon. Many host lattices have been studied for up-conversion processes. Up to now the most efficient green phosphor hosts are $\alpha\text{-NaYF}_4$, YF_3 , and $\text{NaLa}(\text{WO}_4)_2$. Extreme chemical purity is needed because ions such as Dy^{3+} and Fe^{2+} quench fluorescence. In regard to crystal structure, it is found that visible emission intensity increases with: 1. longer Er^{3+} -anion distances, 2. higher valence of the cations in the host lattice, and 3. lower symmetry around the Er^{3+} ion. These conditions result from the fact that in rare-earth ions the first-order selection rules are removed by low-symmetry crystal fields and that longer interatomic distances and weak interactions tend to reduce phonon frequencies.

8. Cathodochromic and Photochromic Materials

Cathodochromic materials [18] are used in cathode-ray storage-display tubes for radar systems and computer terminals. An absorption band in the material is generated by electron-beam bombardment, and the coloration thus obtained is reversible either by bleaching with light or by heating. Resolution is determined chiefly by the spot size of the electron beam, and the contrast ratio is independent of the light intensity used to view the color change.

Electron-beam induced color-centers were used in cathode-ray tubes as early as 1940. Irradiating KCl with electrons produces F-centers with absorption bands in the middle of the visible spectrum. Potassium chloride was unsuccessful in cathode-ray tube displays because the amount of coloration was far too small. Radar displays met with greater

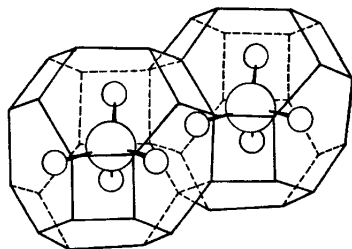


Fig. 53. Schematic diagram of sodalite cage structure. The halogen ions are the large balls in the center of the cage and the small balls are the Na ions. The solid and dashed lines define the aluminosilicate cages. Al and Si atoms (not shown in the figure) alternate at the intersections of the lines. Each line segment passes through an O atom, but does not intersect the atomic center

success because KCl is better suited to storage-display applications. Persistence of the image can be matched to the requirement set by the radar sweep rate, eliminating flicker. But, dark-trace tubes with evaporated KCl screens still suffered from low contrast, and from fatigue after repeated use.

Superior cathodochromic properties are found in CaTiO_3 (perovskite) and in $\text{Al}_6\text{Si}_6\text{O}_{24} \cdot 2\text{Na}_4\text{Cl}$ (sodalite). Calcium titanate screens doped with Fe and Mo show efficient optical bleaching without fatigue, but the contrast is too low for many display applications. S- and F-doped sodalites have far better contrast ratios, but when operated at high contrast, thermal erasure is required.

Sodalite has a cage-like structure consisting of interconnected cuboctahedra (Fig. 53). The aluminosilicate cages contain chlorine ions coordinated tetrahedrally to four sodium ions. Several types of dopants produce coloration. Cl^- can be replaced by halogens such as Br^- and I^- , or by S^{2-} , Se^{2-} and Te^{2-} with halogen vacancies in adjacent cages. The amount of nonstoichiometry and crystallite size are important parameters influencing the cathodochromic properties.

There are two coloration mechanisms in sodalite, both resulting in the formation of F centers with an electron trapped at a halogen vacancy. In *optical-mode coloration*, the electron beam creates hole-electron pairs. Holes combine with S^{2-} to form S^- while electrons are trapped at nearby halogen vacancies to form F-centers. Irradiated regions darken because visible photons are absorbed in raising trapped electrons from the ground state to excited states. Higher energy photons bleach the darkened regions by liberating trapped electrons from the F-centers, returning the electrons to sulfur donors.

Thermal-mode coloration in sodalite involves double-defect cages, which are missing both a Na^+ and a halogen ion. When a high energy electron enters sodalite, there is a good possibility it will eject a Na^+ ion from a complete cage, transferring it to a double-defect cage. In this way a double defect cage and a complete cage are converted into two single vacancy cages, one with a cation vacancy and the other with an anion vacancy. The latter becomes an F-center when it traps one of the many secondary electrons created by the cathode rays. No dopants are required for this process. Bleaching takes place *via* ionic diffusion as the two single-cage defects recombine. This type of coloration must be bleached thermally since high temperatures are required to promote ionic diffusion.

The F-center absorption wavelength is linearly related to the size of the sodalite cages. Si can be replaced by Ge and Al by Ga to increase the cage size.

Cathodochromic devices are well-suited to storage and display with a gray scale and high resolution. Storage times range from a few seconds to many months. Under normal operating conditions, optically erasable cathodochromic tubes have a useful storage time of about a minute; while that of thermal-erase tubes is practically infinite. Applications for cathodochromic materials include high-resolution display panels, radar systems, narrow band width image transmission systems, and image storage and retrieval systems.

Photochromic glasses with reversible coloring have been prepared by Corning Glass Works. The glass darkens under exposure to sunlight making it ideal for sunglasses and window panes. The photochromic process involves several reactions with silver ions migrating through the glass to form crystals with Cl^- and F^- . Small silver halide crystals are developed in certain glasses by special heat treatment. A typical composition is SiO_2 63 wt-%, Na_2O 10 wt-%, Al_2O_3 10 wt-%, B_2O_3 16 wt-%, with about 0.4% Ag and an equal amount of Cl and F [19].

9. Optical Activity

When plane-polarized light enters a crystal it divides into right- and left-handed circularly polarized waves. If the crystal possesses handedness, the two waves travel with different speeds, and are soon out of phase. On leaving the crystal, the circularly polarized waves recombine to form a plane polarized wave, but with the plane of polarization rotated through an angle αd . The crystal thickness, d , is in mm, and α is the optical activity coefficient expressed in degrees/mm. The polarization

vector of the combined wave can be visualized as a spiral, turning α° per mm path length in the optically-active medium. Because of the low symmetry of the spiral, optical activity is not observed in many high symmetry crystals. Point groups possessing a center of symmetry or more than two mirror planes are inactive.

In relating α to crystal chemistry it is convenient to divide optically-active materials into two categories [20]: those which retain optical activity on melting, and those which do not. It has long been known that optically-active solutions crystallize to give optically-active solids. This follows from the fact that molecules lacking mirror or inversion symmetry can never crystallize in a pattern containing such symmetry elements. Thus one way of obtaining optically-active materials is to begin with optically-active molecules, as in rochelle salt, tartaric acid or cane sugar. Few of these crystals are very stable, however, and the optical activity coefficients are usually small, typically $2^\circ/\text{mm}$.

The same is true of many inorganic solids, though they are seldom optically active in the liquid state. For NaClO_3 and $\text{MgSO}_4 \cdot 7\text{H}_2\text{O}$, α is about $3^\circ/\text{mm}$. Quartz and selenium, however, have coefficients an order of magnitude larger (Fig. 54), showing the importance of spiral structures to optical activity. Both compounds crystallize as right- and left-handed forms in space groups $P3_12$ and $P3_22$, with spirals about the trigonal screw axes.

Quartz contains nearly regular SiO_4 tetrahedra with Si-O distances of 1.61 Å and O-O distances as short as 2.60 Å. Levorotatory quartz belongs to space group $P3_12$ and contains right-handed spirals; enantiomorphic dextrorotatory quartz crystallizes in $P3_22$. Trigonal selenium also contains spiral chains (Fig. 55). Se-Se distances along the chain are 2.32 Å, much less than the shortest distance between atoms in neighboring chains, 3.46 Å.

When a solid contains spirals of one-handedness it is obvious why right- and left-circularly polarized light travel at different speeds causing optical activity. The wave with the same handedness as the structure does more work because the electric vector continuously polarizes matter, and the wave therefore travels slower. There are several ways to enhance this effect to obtain larger activity coefficients. Atoms with large polarizabilities can be expected to give larger interactions with the light waves. Since polarizabilities increase near an absorption edge, the optical activity coefficients also increase (Fig. 54). Another important parameter is the pitch of the spiral. In most inorganic crystals the spiral pitch is 10 Å or less, far smaller than the wavelength of visible light. Helices with larger pitches give greater rotatory power, as has been demonstrated with liquid crystals. Cholesteryl liquid crystals give coefficients as large as $10^{50}/\text{mm}$.

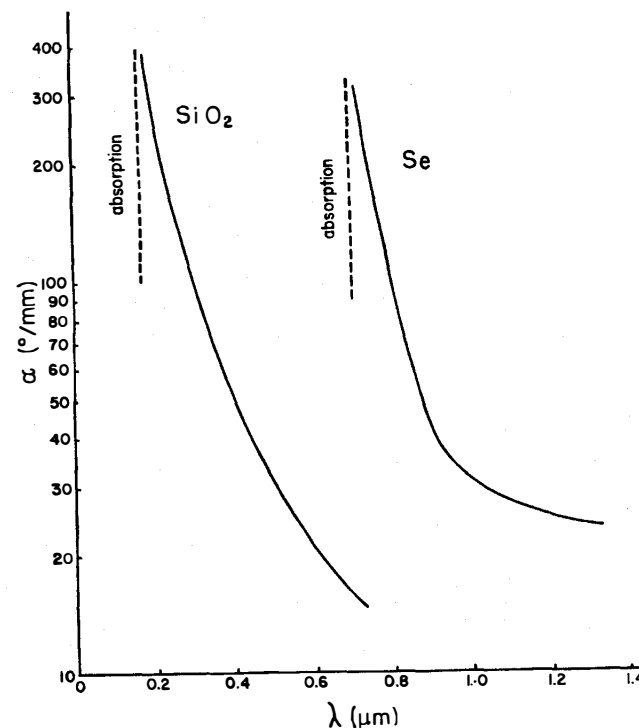


Fig. 54. Dispersion of the principal optical-activity coefficient of quartz and selenium. The plane of polarization is rotated in opposite directions for the two enantiomorphs

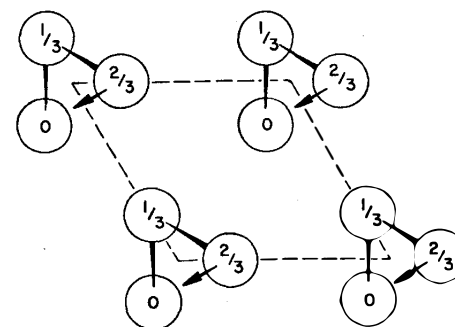
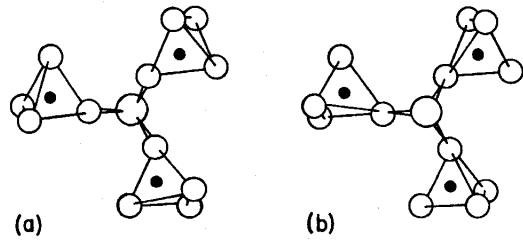


Fig. 55. Selenium structure with spiral chains normal to the paper



$\text{Pb}_5\text{Ge}_3\text{O}_{11}$.
1 and right-
evering the
ses both the
[22]

Lead germanate, $\text{Pb}_5\text{Ge}_3\text{O}_{11}$, is an unusual crystal which exhibits reversible optical rotatory power. Below 177°C , it is a ferroelectric in which a dextro-levo conversion accompanies reversal of the spontaneous polarization [21]. The rotatory power is $5^\circ 35'/\text{mm}$ at 6328 \AA , large enough for opto-electronic devices. The molecular origin of the effect is illustrated in Fig. 56. In the high-temperature prototype structure, some of the lead ions in lead germanate are coordinated to six oxygens arranged in a trigonal prism. On transforming to the ferroelectric state, the lead ions displace forming short bonds to three oxygens and creating spontaneous polarization. Each oxygen is bonded to germanium, and the GeO_4 tetrahedra are twisted when Pb displaces. The twists impart a handedness to the molecular configuration, causing optical activity. The molecular groups resemble a three-bladed airplane propellor of variable pitch [22].

10. Photoelasticity

The change in refractive indices with mechanical stress, the photoelastic effect, is widely used in analyzing stress patterns in engineering components of complicated shape. It is also important in acousto-optic devices, optical switches, modulators and scanners, in which ultrasonic waves modulate the refractive index, producing an optical grating [23].

Materials with sizeable photoelastic coefficients are needed to enhance the interaction between mechanical strain ϵ and refractive index n . Changes in the indicatrix are given by

$$\Delta\left(\frac{1}{n^2}\right) = p \epsilon. \quad (1)$$

These quantities are actually tensors but are treated as scalars in the following discussion which is concerned with the magnitudes of the photoelastic coefficients p , and not their variation with direction.

Unlike the electro-optic effect, photoelasticity occurs in all symmetry classes and is *not* a null property. The maximum values of p measured for a number of materials ranges between 0.1 and 0.6. Photoelastic coefficients are dimensionless because strain and refractive index are dimensionless. For most oxides and halides, $p_{\max} \approx 0.2$ [23].

To gain a clearer understanding of the effects of stress on refractive index, consider the effect of hydrostatic pressure on a cubic crystal. The Lorenz-Lorentz equation is valid for many cubic materials:

$$\frac{n^2 - 1}{n^2 + 1} = K N \alpha. \quad (2)$$

K is a proportionality constant, N the number of molecules per unit volume, and α the polarizability per molecule. Differentiating with respect to the density ρ , gives

$$\frac{dn}{d\rho} = \frac{(n^2 - 1)(n^2 + 2)}{6n\rho} \left(1 + \frac{\rho}{\alpha} \frac{d\alpha}{d\rho}\right). \quad (3)$$

Combining Eqs. (1) and (3) leads to

$$p_{\text{average}} = \frac{(n^2 - 1)(n^2 + 2)}{3n^4} \left(1 + \frac{\rho}{\alpha} \frac{d\alpha}{d\rho}\right). \quad (4)$$

It is apparent from Eqs. (3) and (4) that the photoelastic coefficients depend on pressure through both the volume and polarizability. As the pressure increases, the atoms are packed closer together causing an increase in the refractive index. Pressure changes may also change the atomic polarizabilities so that $d\alpha/d\rho \neq 0$. When a solid is compressed, the electrons are bonded more tightly, decreasing the polarizability. Thus the term $d\alpha/d\rho$ appearing in Eqs. (3) and (4) is negative, and the resulting change in refractive index opposes the effect of a volume decrease. The two effects are of the same order of magnitude, so that the refractive index *increases* with pressure in some oxides (Al_2O_3), decreases in some (MgO), and is almost constant in others ($\text{Y}_3\text{Al}_5\text{O}_{12}$) [24]. Because of the compensatory nature of these two effects, there appears to be little hope for finding large photoelastic coefficients in most materials.

Possible exceptions are compounds containing lone pair cations and materials with large piezoelectric coupling coefficients. The latter may produce internal electric fields when a strain is applied, and enhance the

photoelastic effect with a strong electro-optic contribution. Lone pair ions are present in α -iodic acid and in lead nitrate, which have unusually large photoelastic constants. When pressure is applied to an ionic compound, the increased orbital overlap causes the charge distribution to become more uniform, decreasing the charge of the anions and increasing that of the cations. In most compounds the decrease in anion polarizability exceeds the increase in cation polarizability, but heavy lone pair cations such as Pb^{2+} have exceptionally large polarizabilities, and the added electron content may result in $d\alpha/dQ$ becoming positive instead of negative. The effects due to volume and polarizability would then add, giving large photoelastic coefficients.

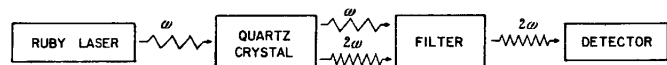


Fig. 57

tent. iting

11. Nonlinear Optical Materials

The linear relation between electric polarization and applied electric field is accurately obeyed even for fairly large fields of 10^5 V/cm. The reason is that the atomic displacements are extremely small, in the range of nuclear sizes—millions of times smaller than the size of atoms. Though nonlinear effects such as electrostriction have been known for some time, it was not until the invention of the laser that sufficiently large electric fields became available to produce sizeable nonlinear effects [25]. The polarization P can be written as a power series in an electric field, where

$$P = \chi E + \xi E^2 + \dots,$$

χ is the linear electric susceptibility, and the higher-order terms lead to nonlinear effects such as second harmonic generation (Fig. 57).

The electric field associated with the incident light is sinusoidal, $E = A \sin \omega t$, and when E is substituted in the expression for P , a power series in $\sin \omega t$ results. The second term is $A\xi \sin^2 \omega t = \frac{1}{2} A\xi (1 - \cos 2\omega t)$, which includes a component of polarization with twice the frequency of the impressed field E . This rapidly oscillating induced dipole moment is the source of second-harmonic light. The intensity of the light depends on the size of ξ , the second order coefficient.

Crystal symmetry is a major contributor to the second-order effect. The one-dimensional polar chain in Fig. 58a illustrates the origin of the

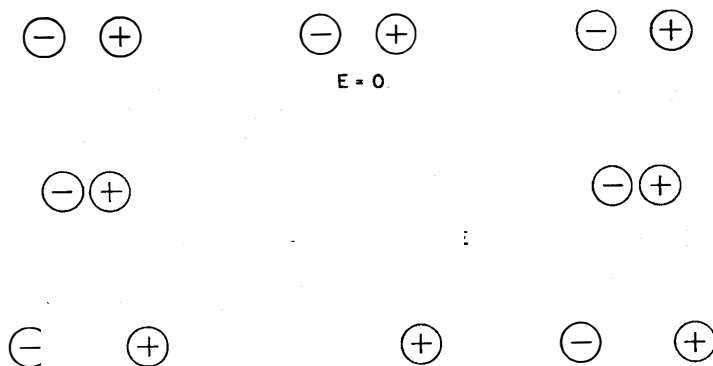


Fig. 58

directed to the left and right, optical effects

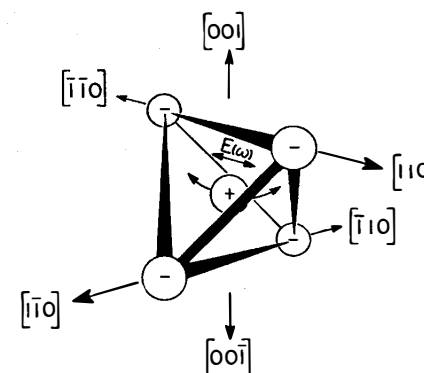


Fig. 58 b. Displacement of a tetrahedrally-coordinated cation in response to an alternating electric field. The path is curved upward because of the attraction to anions, giving rise to optical nonlinearity

quadratic term. When the applied field is directed to the left, the ions are in very close contact and the displacements will be small because of short range repulsive forces. These forces do not oppose motion in the opposite direction, so that fields directed to the right give larger motions and larger polarizations. A centric chain does not show this effect. Such a chain can give rise to odd-order terms producing saturation but not to even power terms in the $P(E)$ relation.

This means that centric crystals are useless as second harmonic generators. In fact, the second harmonic experiment is a good test for the existence of inversion symmetry. A strong signal is proof of the absence of a center of symmetry because intense SHG is possible only in acentric crystals. One approach to obtaining acentric crystals is the use of acentric molecules with permanent distortions caused by non-bonded electrons. HIO_3 and LiIO_3 contain IO_6 octahedra with large trigonal distortions and are promising nonlinear optical materials.

Quartz is acentric but is not an outstanding second harmonic generator. The best SHG materials have large refractive indices. According to MILLER's rule [26] the SHG coefficients are proportional to $(n^2 - 1)^3$. Increasing n from 1.5 to 2.5 increases ξ by two orders of magnitude. Thus the titanates and niobates are excellent nonlinear optical materials, and narrow band gap semiconductors are also outstanding because of the inverse relation between n and E_g . InSb has a refractive index of 3.5 at 1.06μ , and the SHG signal is more than a thousand times greater than quartz.

The physical origin of optical nonlinearity can be demonstrated with the zincblende structure. In cubic ZnS, each atom is tetrahedrally coordinated to four nearest neighbors of the opposite charge. The tetrahedral edges are parallel to $\langle 110 \rangle$ directions as shown in Fig. 58b. Consider an electromagnetic wave of frequency ω propagating through the crystal in a $[110]$ direction and polarized alternately along $[110]$ and $[1\bar{1}0]$. The ion at the center of the tetrahedron responds to the electric force by initially moving in the direction of the field. But as the ion leaves the equilibrium position in either the $[110]$ or $[1\bar{1}0]$ direction, it is attracted to the negatively charged ions above as the distance to one of these ions decreases. The result is a displacement which tends to follow the electric vector of the light wave but is curved upwards at the extremes.

Two components can be identified when this curved motion is observed along the direction of the light beam. One is a motion along $[110]$ parallel to the driving field E and vibrating with the same frequency ω . But, there is also a small component of displacement parallel to $[001]$ and vibrating at frequency 2ω . For every cycle of $E(\omega)$, the ion will twice reach maximum excursion along $[001]$. Thus a light wave traveling along $[110]$ and polarized parallel to $[110]$ generates a second harmonic polarized along $[001]$.

Birefringence can be useful in SHG materials. Greatly amplified harmonics are possible if the velocities of the fundamental and harmonic waves are made equal. This kind of phase matching is possible if the difference in refractive index due to dispersion can be matched by birefringence. Noncritical phase-matching in uniaxial crystals is the best

because energy flow directions are also coincident, thereby eliminating walk-off problems.

Optical images can be stored in crystals as phase gratings which can be written and read by laser beams. The holograms are written by liberating free charge carriers from traps with incident light. Electrons diffuse from the illuminating regions to the darker regions producing space-charge electric fields which in turn modulate the refractive index through the electro-optic effect. The refractive index of the crystal is, therefore, modulated according to the optical image, forming a phase grating. In crystals such as LiNbO_3 the image can be fixed by gentle heating, allowing positive ions to diffuse to the regions of negative space charge, neutralizing the local electric fields. After cooling the crystal, the field is restored and the phase grating fixed by uniform illumination. This makes the electron configuration uniform but leaves behind a non-uniform ion distribution which forms the phase grating.

References for Chapter V

1. WEMPLE, S., DIDOMENICO, D.: J. Appl. Phys. **40**, 735 (1969).
2. LARSEN, E.S., BERMAN, H.: The Microscopical Determination of the Non-opaque Minerals, 2nd ed. Washington, D.C.: U.S. Geological Survey, Bull. 848, 1934.
3. MAURER, R.D.: Proc. I.E.E.E. **61**, 452 (1973).
4. ZHDANOV, G.S.: Crystal Physics. New York: Academic Press 1965.
5. BRAGG, W.L.: Proc. Roy. Soc. (London) **A105**, 16, 370, **A106**, 346 (1924).
6. BROFMAN, O., STEINBERGER, I.T.: Phys. Rev. **143**, 501 (1966).
7. GOLIGHTLY, J.P.: Canad. Min. **10**, 105 (1969).
8. PARSONS, W.F.: J. Appl. Optics **11**, 43 (1972).
9. SPARKS, M., CHOW, H.C.: J. Appl. Phys. **45**, 1510 (1974).
10. FARRELL, E.F., NEWNHAM, R.E.: Am. Mineralogist. **50**, 1972 (1965).
11. TOWNSEND, M.G.: J. Phys. Chem. Solids **31**, 2481 (1970).
12. KISS, Z.J., PRESSLEY, R.J.: J. Appl. Optics **5**, 1474 (1966).
13. DUKE, C.B., HOLONYAK, N.: Phys. Today, p. 23, Dec. 1973.
14. BLASSE, G.: Mat. Res. Bull. **3**, 807 (1968).
15. WABER, J.T., CROMER, D.T.: J. Chem. Phys. **42**, 4116 (1965).
16. BLASSE, G., BRIL, A.: Philips Tech. Rev. **31**, 304 (1970).
17. AUGEL, F.E.: Proc. I.E.E.E. **61**, 758 (1973).
18. FAUGHNAN, B.W., GOROG, I., HEYMAN, P.M., SHIDLOVSKY, I.: Proc. I.E.E.E. **61**, 927 (1973).
19. ARMISTEAD, W.H., STOOKEY, S.D.: Science **144**, 150 (1964).
20. LOWRY, T.M.: Optical Rotatory Power. New York: Dover Publications 1964.
21. IWASAKI, H., SUGII, K.: Appl. Phys. Lett. **19**, 92 (1971).
22. NEWNHAM, R.E., CROSS, L.E.: Endeavour **33**, 18 (1974).
23. PINNOW, D.A.: Proc. I.E.E.E. QE-6, 223 (1970).
24. KIRK, J.L., VEDAM, K.: J. Phys. Chem. Solids **33**, 1251 (1972).
25. BERGMAN, J.B., KURTZ, S.K.: Mat. Sci. and Eng. **5**, 235 (1969).
26. MILLER, R.C.: Appl. Phys. Lett. **5**, 17 (1964).